RSC Advances

ROYAL SOCIETY OF CHEMISTRY

www.rsc.org/advances

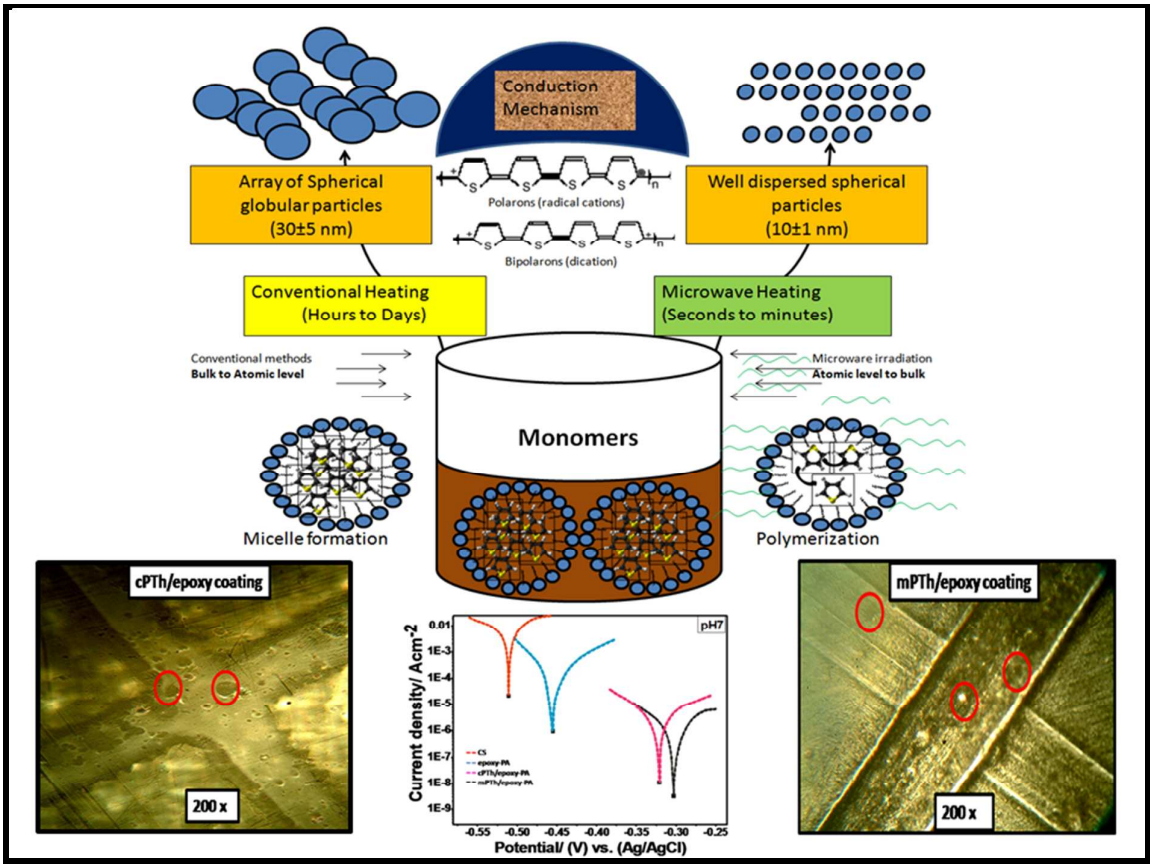

The time and energy efficient microwave synthesis of nano polythiophene provides higher yield, smaller particle size, superior physico-mechanical properties and promising corrosion inhibition properties as compared to conventional synthesis.

Title: Influence of microwave irradiation on various properties of nanopolythiophene and their anticorrosive nanocomposite coatings

Names of Authors

Neha Kanwar Rawat

Research scholar

Materials Research Laboratory, Dept of Chemistry

Jamia Millia Islamia, New Delhi. 110025.

Email: neharawatjmi@gmail.com

Anujit Ghosal

Research scholar

Materials Research Laboratory, Dept of Chemistry

Jamia Millia Islamia, New Delhi.

Email: anuj.ghosal@gmail.com

***Corresponding Author**

*Prof. Sharif Ahmad

Materials Research Laboratory, Dept of Chemistry

Jamia Millia Islamia, New Delhi. 110025.

Email: sharifahmad_jmi@yahoo.co.in

Tel no. +91 11 26827508

Fax: +91 11 26840229

Abstract:

Nano Conducting polymers (CPs) dispersed polymer hydrophobic coatings are considered to be a new generation coating system. They have promising applications in the area of anticorrosive coatings and have proved to be an effective alternative to the toxic phosphate–chromate based coatings. In view of this, for the first time, we report here, the effect of microwave (MW) irradiation on various properties of Polythiophene (PTh) and their comparison with conventionally polymerised nano PTh (cPTh). The effect of MW irradiation on the morphology, size, solubility and electrical properties are investigated with the help of TEM, SEM, CV and four probe conductivity measurements. The synthesis has been carried out in aqueous medium, as it is green, renewable, environmental friendly and free from harmful VOCs. The nano PTh dispersed epoxy-polyamide (PA) nanocomposite coatings are developed on carbon steel (CS). The mPTh-epoxy-PA shows superior flexibility, gloss, adhesion, impact and scratch resistance properties than that of cPTh-epoxy-PA nanocomposite coatings The salt spray test and potentiodynamic polarization (PDP) studies on these coatings reveal, that the mPTh-epoxy-PA nanocomposite coatings, show superior anticorrosive properties (E_{corr}/I_{corr} : -0.30301V/3.1587E-09 Acm^{-2}) than cPTh-epoxy-PA (-0.32138 V/ 1.1003E-08 Acm^{-2}) and epoxy-PA (-0.45505 V/ 9.3862E-07 Acm^{-2}) coatings. The morphology of corroded and uncorroded coatings, are analysed by SEM/EDAX. The promising physico-mechanical properties and corrosion protection performance of mPTh-epoxy-PA nanocomposite coatings highlighted the potential of MW techniques for the synthesis of CPs.

Keywords: polythiophene nanoparticles, microwave and conventional emulsion synthesis, electrochemical corrosion, potentiodynamic polarization, cyclic voltammetry

1. Introduction:

Conducting polymers (CP) like Polyaniline, Polypyrrole, Polythiophene (PTh) and their derivatives are considered to be a fair class of materials. Owing to the presence of conjugated pi-electrons, they exhibit promising electronic, magnetic and optical properties.[1-5] It has been observed that the synthesis techniques, morphology and size of the conducting polymers influence the properties and application of these polymers.[3, 6, 7] The key areas of their applications are sensors,[8] catalysis,[9] solar cells,[10] supercapacitors,[11] electrochromic luminescent shielding materials,[10] antistatic coatings and corrosion inhibitors.[12]

Literature reveals that the effect of synthesis methods on properties and characterization of un-substituted PTh has scarcely been investigated in comparison to other conducting polymers like Polyaniline,[13-15] Polypyrrole[16, 17] and their derivatives. Polymerization of thiophene (Th) in general is carried out by three different ways: (i) Electro-polymerization, (ii) Metal catalyzed coupling reactions and (iii) Chemical oxidative polymerization.[18] Lee et al.[19] have reported the synthesis of PTh nanoparticles via ferric chloride/hydrogen peroxide ($FeCl_3/H_2O_2$) acting as catalyst and oxidant, while the effect of concentration of oxidant, reductant and catalyst on the morphology of PTh was investigated by Liu et al.[20] The synthesis of PTh in anhydrous media with cationic, anionic and non-ionic surfactants and their influence on morphology, conductivity and thermal stability were studied by Gok et al.[21] The un-substituted PTh using binary organic solvents was prepared by Jeon et al.[22] However, in these synthesis some short comings are observed like higher reaction time, lack of monomer reactivity, poor yield, use of organic solvents, production of volatile organic components (VOC`s), causing health hazards and use of multi-reagents in a single reaction system (like sodium thiosulphate, ammonium persulphate, dodecyltrimethylammonium

bromide (DTAB) and Tween 80**)** has been associated with conventional synthesis techniques.[22-24]

Among the newly developed synthesis techniques, MW technique has been found to be highly chemical/energy efficient, time saving and eco-friendly in nature. [25, 26, 27,53] A scant literature is available on the MW assisted synthesis of substituted PTh as reported by McCollouch et al in case of polyterthiophenes.[24] Melluci et al reported synthesis of PTh oligomers via Suzuki coupling reactions. [28] However, to the best of our knowledge the MW synthesis of substituted PThs has been reported, it is important to mention here that till date no reference is available on the MW synthesis of unsubstituted PTh in aqueous medium. Moreover, the MW synthesis of unsubstituted PTh in aqueous medium, which is renewable and green in nature as during the synthesis no harmful VOCs are produced.

Usually corrosion causes disastrous losses for any infrastructure like bridges, ships, machinery etc, which involves the use of metals and their alloys. Therefore, protection of materials from such undesirable deterioration is of prime importance because of its direct or indirect effect on the economy and human life.[29] Polymer coating is considered to be an effective, simple and an economical method in nature as compared to other corrosion protection techniques[29] Literature reveals that, for the improvement in the protection efficiency of polymer coatings, further studies on the role of dispersion of organic nano-conducting polymers, inorganic nano-particles like metals and their oxides (Ti, Fe, TiO_2, Fe_3O_4 etc.)[30] in insulating polymer matrix are essentially required. CPs have recently proved to be an effective alternative to the conventional hazardous phosphate–chromate pretreatments[31] and they find promising application in the area of hydrophobic anticorrosive coatings. The dispersion of nano CP due to their better compatibility with organic matrices induces good barrier action involving redox protection mechanism that provides them an

extra edge.[32] The interest in these polymers also developed due to the fact that they can exist in different oxidation states and can easily be converted from one state to another.[33]

The aim of present work is the first attempt to investigate the comparative study for the physico-mechanical properties and anti-corrosive performance of PTh dispersed epoxy nanocomposite synthesized by MW method (mPTH-epoxy-PA) with that of conventionally synthesized epoxy nanocomposite coatings (cPTh-epoxy-PA).

2. EXPERIMENTAL SECTION

2.1. Materials. Thiophene monomer (Th) (C_4H_5S, Mol. Wt. 84.14, Spectrochem, India), Cetyltrimethylammonium bromide (CTAB) (Spectrochem, India, Minimum Assay 99 % M. range-248-250 ^oC, $C_{19}H_{42}Br$ N, Mol. Wt. -162.21), Ferric Chloride anhydrous ($FeCl_3$) (s.d fine chem., India), Potassium chloride, Diglycidyl ether of bisphenol A Epoxy (DGEBA, D.E.R 332, epoxy equivalent 180–185, sp.gr. 1.2306, refractive index 1.5685, viscosity about 10,000 CP) was procured from DOW Chemicals, Benzoyl peroxide (Qualigen, India), polyamide as curing agent (Aradur HY 840-1 EN, CAS No. 112-24-3, amine number 500-580), Methanol (Sigma Aldrich, 97 %) and millique water. All the chemicals were of analytical grade and were used without further purification.

2.2. Synthesis of PTh using conventional emulsion polymerization technique (cPTh).[21]

Thiophene (Th) monomer (1.0 g) was dissolved slowly in a micellar solution (30 ml of millique water containing 10 ml of 3.38 mmolar CTAB solution) in a three neck flask containing magnetic bar on a magnetic stirrer. Freshly prepared $FeCl_3$ solution (55.0 mmolar) was added to this micellar reaction mixture, which act as an oxidant and catalyst to initiate the polymerization of Th monomer. The polymerization reaction was conducted under constant stirring at 298K temperature and atmospheric pressure condition for a period of 24 h. The progress of the reaction was monitored by the change in the colour of the reaction adduct (colourless to light brown). On the appearance of dark brown colour, the reaction was

stopped and the precipitated polythiophene (cPTh) was filtered using Buchner funnel. The filtered precipitate was thoroughly washed with distilled water and acetone to remove the presence of any un-reacted low molecular weight oligomers and unwanted reagents. The precipitate was dried in vacuum oven under reduced pressure (25 Hg) at 50 ^{o}C for 48 h. The yield % of the vacuum dried cPTh particles was found to be 55 % and was used for further characterization.

2.3. Synthesis of PTh by microwave technique (mPTh). Microwave synthesis was performed using Erlenhymer flask at constant power of 360 W for 120 s in domestic microwave oven (LG, MW frequency 2500 MHz, power source 230 V, (~ 50 Hz), energy output 800 W, input power 1200W). The reaction mixture containing Th, CTAB, $FeCl_3$ and millique water in same proportion as was used in conventional surfactant assisted synthesis of cPTh. The reaction mixture was transformed into Erlenhymer flask followed by MW irradiation for a period of 120 s. The resulting solution was kept aside to observe the change in colour of MW irradiated solution. A brown colour precipitate of mPTh particles formed was filtered. The filtrate was thoroughly washed with distilled water and acetone to **remove** the possibility of any low molecular weight oligomers and unreacted reagents followed by drying in vacuum oven at reduced pressure (25 Hg) at 50 ^{o}C for 48 h. The yield % of finally dried mPTh particles was found to be 68% and the same was used for further characterization.

Synthesis of mPTh and cPTh were repeated under same experimental conditions at least three times to check the reproducibility of the results, the optimisation studies are provided in supporting information 1, Table S1.

2.4 Formulation of cPTh and mPTh dispersed epoxy nano-composites. The cPTh-mPTh–epoxy nano-composites were prepared by solution blending of 5 wt. % of cPTh and mPTh nano-particles in epoxy using ethyl methyl ketone as solvent. The ultrasonication of mPTh

into epoxy matrix was carried out for 20 min followed by mechanical stirring for 5 h at room temperature, which resulted in the formation of a homogeneous solution having completely dispersed nanoparticles within the matrix. Similarly, cPTh nanoparticles were dispersed in epoxy matrix by ultra-sonication for 30 min followed by mechanical stirring for 5 h. The resulted nano-composites were kept under observation for fortnight to see any phase separation. However, there was no phase separation observed. Their coatings (average thickness 130 μm) were prepared by brush technique on finely polished CS strips of standard sizes using the mixture of cPTh-mPTh dispersed epoxy and PA (35 wt. %) using EMK as solvent.

2.5. Characterization. FTIR spectra of cPTh and mPTh were analyzed on PerkinElmer 1750 FT-IR spectrophotometer (PerkinElmer Instruments, Norwalk, CT) in the form of KBr pellets. The particle size and surface morphology was analyzed using Transmission electron microscopy (TEM), model Morgagni 268-D TEM, FEI, USA operated at an accelerated voltage of 120 kV. The crystal structure and phase purity were investigated on Philips X-ray diffractometer model Philips W3710 using Cu Kα radiation. UV–visible spectra were taken on Perkin-Elmer-LAMDA-ez-221 to determine the conjugation and nano nature of these particles. Thermogravimetric analysis (TGA) was performed using the SII EXSTAR 6000 thermal analyzer (Japan) in the range of 40 ^{o}C to 800 ^{o}C under nitrogen atmosphere at 10 ^{o}C/min flow rate, to study the thermal stability of cPTh and mPTh. BET analysis was carried out with the help of Quanta Chrome instrument (model NOVA 2000e USA) using nitrogen gas to determine the surface area of nanoparticles. The redox behavior of thin films of mPTh and cPTh nanoparticles on the surface of ITO glass, were analysed using potentiostat, (model Autolab type III with FRA unit (μ3AVT 70762, Netherlands). The thin films on the surface of ITO glass were used as working electrode, Ag/AgCl as reference electrode and Pt as auxiliary electrode. The conductivity was measured by the standard four probe method using

a Keithley DMM 2001, the EG and G Princeton applied research potentiostat model 362 was used as a current source. Before all electrochemical measurements, the carbon steel specimens (having composition in wt %: 2.87% C and 97.13% Fe [34] were polished successively with different grade of emery papers 600–800–1000 grade. The polished specimens were washed thoroughly with double distilled water, degreased with methanol and acetone, dried at room temperature. The epoxy-PA, cPTh-epoxy-PA and mPTh-epoxy-PA nano composite were applied by brush on the CS strips (70×30×1 mm^3) to prepare their coatings (of thickness 130) for the determination of specular gloss at 45^o by a gloss meter (model RSPT-20, digital instrument Santa Barbara, CA). The scratch hardness (BS 3900), bend test on 1/8" inch conical mandrel (ASTM D 3281-04), cross-hatch test (ASTM D3359) and methyl ethyl ketone (MEK), solvent resistance test (ASTM D5402) and impact resistance (IS: 101 par 5/sec-31988) were conducted. Corrosion resistance performance of epoxy-PA, cPTh-epoxy-PAand mPTh-epoxy-PA on CS specimens were evaluated by potentiodynamic polarization measurements in various NaCl (3.5% NaCl) solutions of different pH (=1, 3, 5, 7, 9, 12 and 14 by adding HCl and NaOH) [12] at room temperature (25^{o}C) using micro Autolab type III with FRA unit (μ3AVT 70762, Utrecht, Netherlands) potentiostat. The Tafel plots in presence of above said corrosive medium were obtained using a three-electrode electrochemical cell (EG&G Albuquerque, NM, flat cell) containing platinum gauze as counter electrode with Ag/AgCl as reference electrode and test specimen (coated and uncoated carbon steel specimens) as working electrode. The test specimens were fitted in electrochemical cell with 1cm^2 area of the sample surface exposed to the corrosive media. The potentiodynamic polarization tests were carried out in the potential range ±100 mV (with respect to OCP) at 0.001 mV/s scan rate. Nova 1.8 software was used for the data fitting and calculation of their results. The Tafel parameters were determined by curve fitting program

available in the said software. Each test was run in triplicate to verify the reproducibility of the data.

3. Results and discussion

3.1. FT-IR analysis. Structural elucidation of the cPTh and mPTh along with their respective epoxy-PA anticorrosive coatings were performed by FT-IR spectral analysis. The FT-IR spectra of cPTh and mPTh nanoparticle have been shown in Fig. 1(a). The characteristic peak of Th ring stretching vibration was observed at 1433 cm^{-1}. The bands at 1043 cm^{-1}, 839 cm^{-1} and 702 cm^{-1} were attributed to C-H, C-S (in-plane and C-H out-of-plane) bending vibration respectively. Apart from all these, the hydroxyl peaks at 3400 cm^{-1} and carbonyl at 1680 cm^{-1} were also found due to the nucleophillic attack of water molecules on positively charged PTh.[22] In case of mPTh, these absorptions bands were more pronounced as compared to cPTh, revealing the formation of well arranged, crystalline, non-agglomerated nano-sized PTh particles as supported by XRD and TEM analysis of the same.

The Fig. 1(b) shows the FTIR spectra's of DGEBA epoxy and PTh dispersed epoxy resin. The main absorption bands of activated epoxy resins are found at 3521 cm^{-1} (ν OH), 1243 cm^{-1} (ν aromatic C-O), 1035 cm^{-1} (ν aromatic C-O) and 913 cm^{-1} (ν epoxy group). The characteristic signals at 3503 cm^{-1} assigned to the C-H stretching of Th, C=C stretching band of Th observed at 1515 cm^{-1}. This revealed the successful dispersion of PTh nanoparticles in epoxy matrix. The dispersion of PTh particles leads to the shifting of the peaks, especially in –OH peak, which can be attributed to the hydrogen bonding and electronic interaction of PTh particles with that of the DGEBA epoxy matrix.

3.2. X-Ray Diffraction analysis. The semi-crystalline structure and phase identification of cPTh and mPTh were illustrated using X-ray diffractogram, as shown in Fig. 2. The XRD of PTh revealed a broad peak at 22^o showing the amorphous nature of cPTh.[6, 19] However, in the case of mPTh, an additional XRD peak at 36.4^o, in addition to a slight hump at 22^o, could

have resulted due to higher electrical conductivity, arising from improved well-ordered structure.[35, 36] Thus, microwave irradiation helps in acquiring more ordered structure in mPTh compared to conventional emulsion polymerized cPTh.

3.3. Cyclic Voltammetry. The cyclic voltammogram of mPTh and cPTh were taken to investigate the oxidation reduction behaviour of both mPTh and cPTh nanoparticles (Fig. 3). The voltammograms were recorded at different scan rates of 10, 20, 50, 100, 200 and 500 mVs^{1} under 0.1 M potassium chloride solution using Ag/AgCl as a reference electrode. The cyclic voltammogram of mPTh showed two anodic peaks (Ep_a) at 0.63 V, 0.90 V and two cathodic (Ep_c) peaks at 0.43 V, 0.79 V. On the other hand, in cPTh anodic (Ep_a) peaks were observed at 0.55 V, 0.90 V and the cathodic (Ep_c) peaks at 0.45 V and 0.80 V. These peaks correspond to the formation of polarons and bipolarons due to the change in a state of polymer.[2] The higher oxidation potential in mPTh revealed that they have better resistance to oxidation than cPTh, which could have resulted due to improved semi-crystalline structure of PTh formed due to MW irradiation. The semi-crystalline structure and improved conductivity could further be concluded due to two oxidation peaks during CV, as the literature revealed that in many instances PTh only showed one broad oxidation peak followed by two corresponding reduction peaks.[23, 37]

The positive potential shift in oxidation potential in mPTh with the increase in scan rate suggested that the electron transfer from the ITO glass to the PTh film may be slow for mPTh.[2] Also, this slow diffusion rate of counter ions and positive anodic potential shift may be attributed to the well-ordered (semi-crystalline nature), compact and smaller uniform particle size of mPTh.[26] Moreover, only one peak was observed in the CV of these materials when curves were recorded with higher scan rates due to participation of a large capacitive current.[13]

The shape of the voltammograms of mPTh and cPTh particles was not influenced by the size, morphology and scan rate. However, oxidation occurs at lower potential due to higher scan rate. The proportionality of current density to the scan rates referred to the reversible behaviour (oxidation/ reduction reaction i.e. formation of radical cations and vice-versa) in both conducting particles (cPTh and mPTh). It has been observed that the mPTh and cPTh nanoparticles exhibit higher oxidation potential then those of electrochemically polymerized PThs.[38-40] The higher oxidation potential of mPTh can be attributed to the highly aligned structure as well as larger surface area. Higher thermal stability of mPTh than cPTh can also be related to their respective oxidation stability (Fig. S1, showing the TGA and its explanation is given in supporting information). However, higher oxidation potential of other reported PTh nanowire may have been resulted due to their morphological effect.[41, 42]

3.4. TEM and SEM/EDAX analysis of cPTh-mPTh nanoparticles. Remarkable changes in the morphology, size, and distribution pattern of particles were observed in the TEM micrograph of the mPTh and cPTh nanoparticles. The micrographs of mPTh (Fig 4(a)) showed the formation of well ordered and uniform nanospheres of *ca.*10 nm size. The SEM image of mPTh (Fig. 4b (i)) also revealed the similar result of formation of spherical particles under MW irradiation. The smaller nano size of mPTh particles can be attributed to fast generation of radical cations, nucleation and polymerization steps[25] during the synthesis under MW irradiation. However, nano-globules (bigger spheres) of *ca.* 30±5 nm size (Fig. 4(a)) were formed in case of conventional surfactant assisted synthesis of PTh. These globules eventually got aligned resulting into a linear array forming a kind of chain network. However, the SEM images (Fig. 4b (ii)) of cPTh showed formation of PTh particulate of spherical and elongated morphology. Indicating the formation of mixed morphology in case of cPTh as compared to mPTh, where formation of uniformly distributed particle having spherical morphology took place.

The TEM image of mPTh dispersed epoxy-PA coating material is given in Fig. S2, in supporting information. Proper uniform dispersion of the mPTh nanoparticles can be seen along with spherical morphology of the mPTh particles. The uniform non-agglomerated dispersion of mPTh in the matrix may be attributed due to the nano-regime size of the particles. The EDAX analysis of the nano PTh showed the presence of various elements of PTh such as S, C in the material (Fig. S3, given in supporting information).

3.5. UV-visible analysis. UV-vis absorption spectra (Fig. 5) of the PTh nanoparticles were recorded in DMSO. The cPTh and mPTh nanoparticles were investigated in various polar and non-polar solvents at room temperature (their results are tabulated and discussed in supporting information, Table S2). The main charge carriers in PTh nanoparticles are polarons and bipolarons.[35, 43] mPTh showed absorption bands at 290 nm, due to π–π* inter band transitions and a broad band in between 520-700 nm, assigned to n–π* transitions in polarons-bipolarons.[22] On the contrary, in cPTh, absorption bands were observed at 260 nm along with a diffused broad band in the range 520-700 nm. The red shift, pronounced UV absorption bands and broad peak observed for mPTh can have resulted due to the increased conjugation in mPTh. The resulting structural regularity of mPTh nanoparticles in comparison to cPTh nanoparticles was responsible for higher conjugation.[35]

3.6. BET studies. The BET analysis of the PTh particles confirmed the porous nature and higher surface area of mPTh particles than cPTh particles. The average surface area of the cPTh nanoparticles was found to be 24.6 m^2g^{-1} having pore size of 8 A˚. However, the mPTh nanoparticles have comparatively higher surface area of 27.14 $m^2\ g^{-1}$ with a higher pore size of 11 A˚. These results were well correlated with that of TEM analysis, as smaller particle size of mPTh had contributed to the higher surface area in mPTh paricles.

3.7. Effect of microwave irradiation on yield strength. The yield for MW synthesized PTh (68 %) was found to be higher than that of conventionally synthesized PTh (55%). The higher

yield in case of mPTh can be attributed to the MW irradiation as it resulted in maximum conversion of monomer to polymer and reduction in the side products in comparison of the conventional synthesis methodology due higher diffusion rate in presence of MW irradiation.[19] Literature revealed that MW irradiation favours reactions involving more polar transition states and repeatedly leading to different product selectivity than the conventional reactions.[44] Further, reactions under MW often proceed more quickly than the conventional thermal reaction with reduced decomposition of the reactants, products or both, thus minimizing the waste and enhancing the yield.

3.8. Conductivity studies. Conductivity measurements of PTh under ambient conditions revealed that the electrical conductivity data were influenced by the morphology, size and mode of synthesis technique.[22] The four probe conductivity studies showed that the conductivity of mPTh and cPTh were found to be 2.1×10^{-2} S/cm and 1.8×10^{-2} S/cm respectively. Higher conductivity of mPTh in comparison to cPTh revealed the presence of higher conjugation, higher crystalline nature and compact structure of the PTh. Li et al.[35] and Yamamoto et al.[36] have synthesized PTh reported its conductivity in the order of 1.1×10^{-4} S/cm and 2.01×10^{-3} S/cm respectively.

3.9 Mechanism of cPTh and mPTh formation. The superior thermal stability, higher oxidation stability and improved conductivity of mPTh than cPTh particles and other improved properties such as solubility, conductivity etc. of mPTh can be attributed to its nano-size. The MW synthesis, involves the use of quantized energy, electromagnetic radiations. The interaction of fast oscillating electric and magnetic fields creates rapid localized heating in the MW reaction assembly.[45] The intrinsic temperature localized around the ions becomes considerably higher, due to non-dissipation of energy in comparison to that of conventional synthesis.[25] These observation may be rationalized on the basis of the formation of a dipolar activated complex from an uncharged adduct in these reactions. The

greater stabilization of more dipolar activated complex by dipole-dipole interactions with the electric field of MWs as compared to the less dipolar adduct, which may reduce the activation energy resulting in the rate enhancement.[24] The MW also plays a significant role in increasing the diffusion rate of Fe^{3+} ion along with Th molecules into the micelles.[19] These combined effects synergistically caused the generation of higher number of radical cations (fast initiation step), which lead to the higher rate of reaction that subsequently enhances the yield of PTh involving very short reaction time.[46]

These results were also supported by Arrhenius law that is the decrease in activation energy and increased probability of molecular impact accelerate the polymerization of monomer.[40] Furthermore, fast crystallization and accelerated homogeneous nucleation due to MW irradiation [45] resulted into smaller particle size (cPTh *ca.* 10 nm size) in comparison to that of conventional synthesis (*ca.* 30 nm size). The schematic presentation of polymerization of Th monomer and synthesis of PTh molecules is given in scheme 1. While, in the case of conventional synthesis, incomplete conversion and poor diffusion of Th monomer in micelles occurred. The dissipation of energy causes the poor generation of radical cations (slow initiation step) involving higher reaction time, resulted in the formation of higher increase in the particle size and reduced yield content of cPTh nanoparticles .

3.10 Physico-mechanical properties of nano-composite coatings*:* Scratch hardness, cross-hatch, impact, bend and MEK rub tests. The physico-mechanical properties of mPTh-epoxy-PA, cPTh-epoxy-PA and epoxy-PA coated CS were carried out to analyse the effectiveness of the prepared coatings against impact, scratch, bending, etc. The scratch hardness values increased from 4.5 to 12 kg in case of epoxy-PA to mPTh-epoxy-PA coating respectively. The increase in scratch hardness was correlated to the uniform distribution of smaller size (nano-size) fillers in epoxy matrix, which lead to the sealing of pores on the coating surface producing locking effect and restricted further indentation.[32] All these are

synergistically responsible for inducing strength to the coating and improving the scratch hardness values of the coatings in the following order mPTh-epoxy-PA >cPTh-epoxy-PA >epoxy-PA.

The strong interactions between the groups like lone pair of sulphur atom and other polar groups present in epoxy, developed an electrostatic interaction with the metal surface, and thus, enhance the adhesion of the coating.[47] The improved adhesion in epoxy, cPTh-epoxy and mPTh-epoxy coating with CS was further analyzed by the cross-hatch test. Fig. 6 represents the optical images of coated CS before and after the cross hatch test. No Pealing or removal of coating was observed after cross hatch test, confirmed strong adhesion of coatings on the metal interface.

Both cPTh-epoxy-PA and mPTh-epoxy-PA coatings passed the impact test. The coatings absorbed the highest limit of impact energy without any crack formation. The dispersion of nano-PTh fillers into the matrix imparts hardness along with plasticity and flexibility to the coatings. Additional flexibility arises from the moieties like polar hydroxyls, oxirane ring and long hydrocarbon chain present in the backbone of the polymer matrix of nanocomposites and due to presence of strong hydrogen bonding between filler and matrix.[32]

The flexibility of the coatings was determined by the bending test using conical mandrel. The coatings were found to be flexible as they bend (1/8``) without any damage or sign of stress /fracture. The data for MEK double rub cycle test of all the coated CS were found higher than 400 cycles. The rub test performance of mPTh-epoxy was best among all the coatings.

3.11 Contact angle measurements: Surface wettability test. The CCD camera images of water droplets on the surface of the bare CS (58^{o}), epoxy-PA, cPTh-epoxy-PA, mPTh-epoxy-PA coated CS coatings are shown in Fig. 7. It was observed that with the decrease in the particle size, the contact angle value increased (74^{o} to 113^{o}) causing an increased surface roughness in nano-scale range, lead to the formation of air pockets within the coating, which

were found to be responsible for increase in contact angle.[32] The increased contact angle values can be attributed to the increased hydrophobic character in coatings, which is considered to be an important parameter required for showing good anticorrosive properties.[48]

3.12 Salt spray test The salt spray test on mPTh-epoxy-PA, cPTh-epoxy-PA, pristine epoxy-PA coated and uncoated CS was conducted for a period of 360 h in 5.0 wt. % NaCl solution. The SEM (Fig. 8(a)) images of epoxy-PA coated CS depicted uniform smooth surface without any pin-holes. The elemental analysis (EDAX) revealed the presence of elemental N, O, C that can be attributed to the interaction behaviour of epoxy and polyamide. The SEM studies of cPTh-epoxy-PA, mPTh-epoxy-PA coated CS before SST showed the development of some roughness, in nm scale (in the form of hills and valleys) due to dispersion of PTh particles. This generates hydrophobic character to the respective coatings.

The uncoated CS was treated as control, neat epoxy-PA, cPTh-epoxy-PA and mPTh-epoxy-PA coatings showed loss in gloss after 120 h, 240 h and 300 h respectively. To further, analyze the morphological effect of SST on mPTh-epoxy-PA coatings, SEM/EDAX (Fig. 8(a) and 8(b)) studies were done for the coated CS before and after exposure to SST. After 360 h of SST the SEM images showed the deposition of salt (NaCl), on the surface of mPTh-epoxy-PA coatings, however, no cleavage of the matrix was visually observed. The EDAX measurement of the coated surface exhibited no metallic iron, only the presence of slight deposition of chloride ions was observed (Fig. 8(d)). The improved corrosion protection performance of nano-composite coatings was synergistically correlated to the generation of hydrophobic surface, barrier and redox protection ability due to dispersed PTh nanoparticles. PTh was also responsible for increased crosslink density and formation of compact coating surface, which did not allow the penetration of corrosive ions to the coating-metal interface.

Thus, improved corrosion resistance performance of the PTh-epoxy-PA coating was observed as compared to that of epoxy-PA coatings.

3.13 Potentiodynamic polarization (PDP) studies: The PDP experiments were performed to quantitatively analyze the anti-corrosion behaviour of cPTh-epoxy-PA, mPTh-epoxy-PA and epoxy-PA coatings. The combined effect of different corrosive species (chloride, hydroxide and hydrogen ions) was investigated using PDP measurements in saline (NaCl) environment at seven different pH. The corrosion current density (I_{corr}) and corrosion potential (E_{corr}) values were obtained by the extrapolation of β cathodic and β anodic curves. The corrosion rate was calculated using equation given below[49] and their experimental data is given in, Table S3 in supporting information. The PDP measurements were performed after coatings were dipped for a period of 6 h to attain the proper stabilization of the system.

$$CR = \frac{W * I_{corr}}{n * F * d}$$

Where, W is the molecular weight, n is the number of electron transferred, F is Faraday constant, d is the density of material and I_{corr} is the corrosion current density of coatings.

The PDP measurements in acidic and basic NaCl media (pH: 1, 3, 5, 9, 12, 14, Fig. 9 (b and c)) demonstrated that the PTh nano particles dispersed nanocomposite coatings inhibited the corrosion of CS in chloride solution by shifting the corrosion potential to the noble direction and reducing the I_{corr} compared to that of epoxy-PA coatings. A positive potential shift in E_{corr} from -0.51073 V for CS, -0.45505 for epoxy-PA to -0.30301 V for mPTh-epoxy-PA coatings in PH 7, NaCl solution revealed the protection ability of PTh in epoxy matrix. The PDP studies of theses coatings and bare CS in NaCl solutions of different pH revealed that the pH of the corrosive medium influence the protective ability of coating. The corrosion inhibition ability of these coatings was found to be lowest at highly basic pH~14 and highly acidic pH = 1.

In the acidic medium (NaCl solution), the presence of H^+ ions in excess induced an aggressive corrosive environment at coating metal interface, through the diffusion of H^+ and Cl^- ions in a self created coating artefacts to the metal surface. Thus causing the fast dissolution of metal ions and its reduction through activation polarisation, which has not allowed the formation of passive oxide film at coating metal interface, suggested by pourbaix diagram[50] leading to the decrease in E_{corr} (-0.61385 V (CS), -0.51424 V (epoxy-PA)) and increase in I_{corr} (8.91E-04 Acm^{-2} (CS), 9.82E-05 Acm^{-2} (epoxy-PA)) values in pH 1 solution.

In basic media Fig. 9(c), with increased OH^- ion concentration the corrosion performance decreased, which can be attributed to the de-protonation and over-oxidization of PTh in the alkaline medium (as in case of other CP like PPy).[51] However, in basic media the environment helped in the protection of CS by accelerating the formation of more stable passive oxide layer, but corrosion is still not fully prevented because of the diffusion of chloride ions, which destroyed the formation of a passive layer.

In highly acidic or basic solution (pH - 1 or pH -14), mPTh-epoxy-PA nano composite coating showed superior corrosion inhibition than that of cPTh-epoxy-PA coatings and far superior than pure epoxy-PA coating. Which can be attributed to the synergistic effects of hydrophobicity, nanosize effect and redox protection, due to the higher potential of CP dispersed nanocomposite coatings.[12] The hydrophobic coatings with reduced surface wet-ability did not allow the diffusion of aqueous corrosive ions through the coating and prevented the accelerating effect of corrosive ions. Smaller particle size of mPTh (*ca.*10 nm) than cPTh (*ca.*30nm), led to the better dispersion in matrix that restricts the indentation and enhanced the interactions with the matrix, which improved the hardness and adhesion of the coatings. Offering improved barrier to the corrosive ions via healing and locking effect.[47] The hydrophobic coatings with reduced surface wet-ability did not allow the diffusion of aqueous corrosive ions through the coating and prevented the accelerating effect of corrosive ions.

Smaller particle size of mPTh (*ca.*10 nm) than cPTh (*ca.*30nm), led to the better dispersion in matrix that restricts the indentation and enhanced the interactions with the matrix, which improved the hardness and adhesion of the coatings. Offering improved barrier to the corrosive ions via healing and locking effect. [47] Generally, CP coatings provide protection through redox and barrier mechanism in different corrosive environment[12]. Further, literature revealed that, CPs formed a passive compact iron/dopant complex layer at the metal-coating interface,[50] which has capability to undergo a continuous charge transfer reaction at the metal-coating interface that provide protection to CS under saline environment. The high oxidation/reduction potential of CP allows iron or carbon steel to be maintained in the passive state, also they reduce the dissolved oxygen in a corrosive medium.[52]

Corrosion rate of metals like Cu, Zn, Al and Cr reduces due to formation of metal oxides of similar potential which protect it from further oxidation however, Fe or carbon steel do not have such ability to form strong adhere oxide films on the surface. In this respect, PTh helps in production of Fe oxide film at the interface of coating and carbon steel substrate through charge transfer.[53] The PTh transfer the charge to the metal surface at coating-metal interface, which oxidised the Fe to Fe^{2+} ion. The PTh regenerated the charge through the reduction of atmospheric O_2. The Fe^{2+} ion reacts with the $-OH^-$ ion and O_2 at coating-metal interface to produce the passive oxide film layer as per scheme 2.

The PDP studies of mPTh-epoxy-PA coatings at different pH in saline environment exhibit the protective performance as per following trend: pH = 7 > 9 > 5>12 >14> 3 > 1. Which reveal that the protective ability of coating significantly reduces at very high and low pH environment, which can be correlated to the breakdown of the passive film formed at coating-metal interface.[12] However, the mPTh-epoxy-PA coating exhibited superior corrosion protective performance among all these systems as well as other such reported systems [49, 52, 53] (Comparative table, Table S4 is given in supporting information).

However, such corrosive environment reduced the corrosion resistance performance of these coatings also, due to the breakdown of passive film or deterioration of the polymeric coatings. The protective performance of PTh coatings on CS followed the sequence: mPTh-epoxy-PA>cPTh-epoxy-PA>epoxy-PA. These results can also be corroborated by comparing the respective E_{corr}, I_{corr} and corrosion rate values for different electrolytes (as given in supporting information, Table S3).

4. Conclusion

The influence of MW irradiation on various properties such as yield, size, conductivity, thermal stability, physico-mechanical and their corrosion inhibiting properties, of PTh and their comparison with conventionally polymerised nano PTh have been reported for the first time. Characterization of mPTh and cPTh revealed that the mPTh nanoparticles have higher yield %, thermal stability, smaller nanoparticle size, and higher conductivity than cPTh nanoparticles. The MW irradiation also leads to generation of monodispersed spherical particles as in case of cPTh mixed morphology was observed.

The mPTh-epoxy-PA nanocomposite coatings have exhibited better physico-mechanical properties, superior corrosion protective performance than cPTh-epoxy-PA and other such reported coatings systems in saline environment at different pH. The higher corrosion protection performance of mPTh-epoxy-PA coatings can be attributed to the smaller size, higher oxidation stability and semi-crystalline structure of mPTh, which induced sealing and healing effect within the coatings. The far superior corrosion protective properties of mPTh-epoxy- PA nanocomposite coatings may provide an opportunity to use them (mPTh-epoxy-PA) as anti-corrosive nano composite coatings on commercial scale.

ACKNOWLEGEMENTS

Neha Kanwar Rawat and Anujit Ghosal are thankful to the University Grants Commission (UGC-BSR) and the Council of Scientific and Industrial Research (CSIR), no:

9/466(0163)/2K13), New Delhi, India, to their financial support for this work. Authors also acknowledge to SAIF centre, All India institute of Medical Science (AIIMS), New Delhi and Panjab University, Chandigarh for TEM and XRD facilities. The authors are grateful for the TGA facility under the UGC, SAP of the Department of Chemistry, JMI, New Delhi, India.

References

1. S. Bhadra, D. Khastgir, N. K. Singha and J. H. Lee, *Progress in Polymer Science*, 2009, **34**, 783-810.
2. E. Grana, D. Katsigiannopoulos, A. E. Karantzalis, M. Baikousi and A. Avgeropoulos, *European Polymer Journal*, 2013, **49**, 1089-1097.
3. A. J. Heeger, *Synthetic Metals*, 2001, **125**, 23-42.
4. A. G. MacDiarmid, *Synthetic Metals*, 2001, **125**, 11-22.
5. H. Shirakawa, *Synthetic Metals*, 2001, **125**, 3-10.
6. Y. W. Lee, K. Do, T. H. Lee, S. S. Jeon, W. J. Yoon, C. Kim, J. Ko and S. S. Im, *Synthetic Metals*, 2013, **174**, 6-13.
7. P. Tian, J. Ye, G. Ning, W. Gong, N. Xu, Q. Zhang and Y. Lin, *RSC Advances*, 2012, **2**, 10217-10221.
8. S. Virji, R. B. Kaner and B. H. Weiller, *The Journal of Physical Chemistry B*, 2006, **110**, 22266-22270.
9. H.-S. Shin and S. Huh, *ACS Applied Materials & Interfaces*, 2012, **4**, 6324-6331.
10. I. Lim, S. J. Yoon, W. Lee, Y.-C. Nah, N. K. Shrestha, H. Ahn and S.-H. Han, *ACS Applied Materials & Interfaces*, 2011, **4**, 838-841.
11. H. P. de Oliveira, S. A. Sydlik and T. M. Swager, *The Journal of Physical Chemistry C*, 2013, **117**, 10270-10276.
12. A. C. C. de Leon, R. B. Pernites and R. C. Advincula, *ACS Applied Materials & Interfaces*, 2012, **4**, 3169-3176.
13. S. Mu and Y. Yang, *The Journal of Physical Chemistry B*, 2008, **112**, 11558-11563.
14. Y. M. Zhou, W. Q. Zhang, L. P. Zhong and D. S. Wang, *J. Magn. Magn. Mater.*, 1995, **145**, L273.
15. B.-J. Kim, S.-G. Oh, M.-G. Han and S.-S. Im, *Synthetic Metals*, 2001, **122**, 297-304.
16. M. Mazur, *The Journal of Physical Chemistry B*, 2008, **113**, 728-733.
17. X. Zhang, J. Zhang, W. Song and Z. Liu, *The Journal of Physical Chemistry B*, 2005, **110**, 1158-1165.
18. J. Zhang and X. S. Zhao, *The Journal of Physical Chemistry C*, 2012, **116**, 5420-5426.
19. S. J. Lee, J. M. Lee, I. W. Cheong, H. Lee and J. H. Kim, *Journal of Polymer Science Part A: Polymer Chemistry*, 2008, **46**, 2097-2107.
20. R. Liu and Z. Liu, *Chinese Science Bulletin*, 2009, **54**, 2028-2032.
21. A. Gök, M. Omastová and A. G. Yavuz, *Synthetic Metals*, 2007, **157**, 23-29.
22. S. S. Jeon, S. J. Yang, K.-J. Lee and S. S. Im, *Polymer*, 2010, **51**, 4069-4076.
23. J. A. Reedijk, H. C. F. Martens, S. M. C. van Bohemen, O. Hilt, H. B. Brom and M. A. J. Michels, *Synthetic Metals*, 1999, **101**, 475-476.
24. S. Tierney, M. Heeney and I. McCulloch, *Synthetic Metals*, 2005, **148**, 195-198.
25. M. R. Gizdavic-Nikolaidis, M. Jevremovic, D. R. Stanisavljev and Z. D. Zujovic, *The Journal of Physical Chemistry C*, 2012, **116**, 3235-3241.
26. M. R. Gizdavic-Nikolaidis, D. R. Stanisavljev, A. J. Easteal and Z. D. Zujovic, *The Journal of Physical Chemistry C*, 2010, **114**, 18790-18796.
27. X. Zhang and S. K. Manohar, *Chemical Communications*, 2006, 2477-2479.

28. M. Melucci, G. Barbarella and G. Sotgiu, *The Journal of Organic Chemistry*, 2002, **67**, 8877-8884.
29. M. Crobu, A. Scorciapino, B. Elsener and A. Rossi, *Electrochimica Acta*, 2008, **53**, 3364-3370.
30. O. u. Rahman and S. Ahmad, *RSC Advances*, 2014, **4**, 14936-14947.
31. S. Ahmad, U. Riaz, A. Kaushik and J. Alam, *Journal of Inorganic and Organometallic Polymers and Materials*, 2009, **19**, 355-360.
32. M. Kashif and S. Ahmad, *RSC Advances*, 2014, **4**, 20984-20999.
33. D. R. Baer, P. E. Burrows and A. A. El-Azab, *Progress in Organic Coatings*, 2003, **47**, 342-356.
34. S. Pathan and S. Ahmad, *Journal of Materials Chemistry A*, 2013, **1**, 14227-14238.
35. X.-G. Li, J. Li and M.-R. Huang, *Chemistry – A European Journal*, 2009, **15**, 6446-6455.
36. T. Yamamoto, *NPG Asia Mater*, 2010, **2**, 54-60.
37. L. Cardenas, R. Gutzler, J. Lipton-Duffin, C. Fu, J. L. Brusso, L. E. Dinca, M. Vondracek, Y. Fagot-Revurat, D. Malterre, F. Rosei and D. F. Perepichka, *Chemical Science*, 2013.
38. Y. A. Udum, K. Pekmez and A. Yıldız, *Synthetic Metals*, 2004, **142**, 7-12.
39. M. Fréchette, M. Belletete, J. Y. Bergeron, G. Durocher and M. Leclerc, *Synthetic Metals*, 1997, **84**, 223-224.
40. G. M. Abou-Elenien, A. A. El-Maghraby and G. M. El-Abdallah, *Synthetic Metals*, 2004, **146**, 109-119.
41. D. H. Park, B. H. Kim, M. K. Jang, K. Y. Bae, S. J. Lee and J. Joo, *Synthetic Metals*, 2005, **153**, 341-344.
42. K. Sakamoto, K. Nakabayashi, T. Fuchigami and M. Atobe, *Electrochemistry*, 2013, **81**, 328-330.
43. J. Fagerström and S. Stafström, *Synthetic Metals*, 1997, **85**, 1065-1068.
44. M. Li, Z. Zuo, L. Wen and S. Wang, *Journal of Combinatorial Chemistry*, 2008, **10**, 436-441.
45. W. C. Conner, G. Tompsett, K.-H. Lee and K. S. Yngvesson, *The Journal of Physical Chemistry B*, 2004, **108**, 13913-13920.
46. S. H. Jhung, T. Jin, Y. K. Hwang and J.-S. Chang, *Chemistry – A European Journal*, 2007, **13**, 4410-4417.
47. R. Arefinia, A. Shojaei, H. Shariatpanahi and J. Neshati, *Progress in Organic Coatings*, 2012, **75**, 502-508.
48. A. K. Dewan, D. P. Valenzuela, S. T. Dubey and A. K. Dewan, *Industrial & Engineering Chemistry Research*, 2002, **41**, 914-921.
49. H. Wei, D. Ding, S. Wei and Z. Guo, *Journal of Materials Chemistry A*, 2013, **1**, 10805-10813.
50. Y. Chen, X. H. Wang, J. Li, J. L. Lu and F. S. Wang, *Corrosion Science*, 2007, **49**, 3052-3063.
51. İ. Çakmakcı, B. Duran and G. Bereket, *Progress in Organic Coatings*, 2013, **76**, 70-77.
52. T. D. Nguyen, T. A. Nguyen, M. C. Pham, B. Piro, B. Normand and H. Takenouti, *Journal of Electroanalytical Chemistry*, 2004, **572**, 225-234.
53. P. J. Kinlen, D. C. Silverman and C. R. Jeffreys, *Synthetic Metals*, 1997, **85**, 1327-1332.

Influence of microwave irradiation on various properties of nanopolythiophene and their anticorrosive nanocomposite coatings

Neha Kanwar Rawat, Anujit Ghosal and Sharif Ahmad*

Materials Research Laboratory, Department of Chemistry, Jamia Millia Islamia,

New Delhi 110025, India.

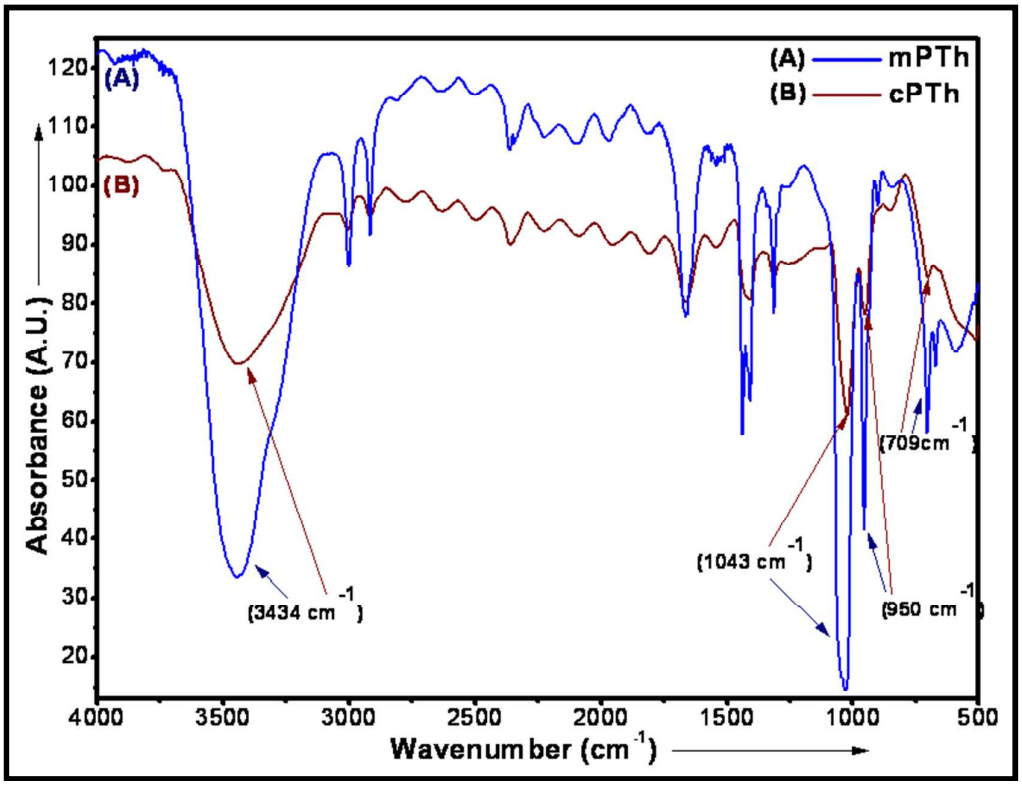

Figure 1(a) FT-IR spectra of (A) mPTh and (B) cPTh nanoparticles.

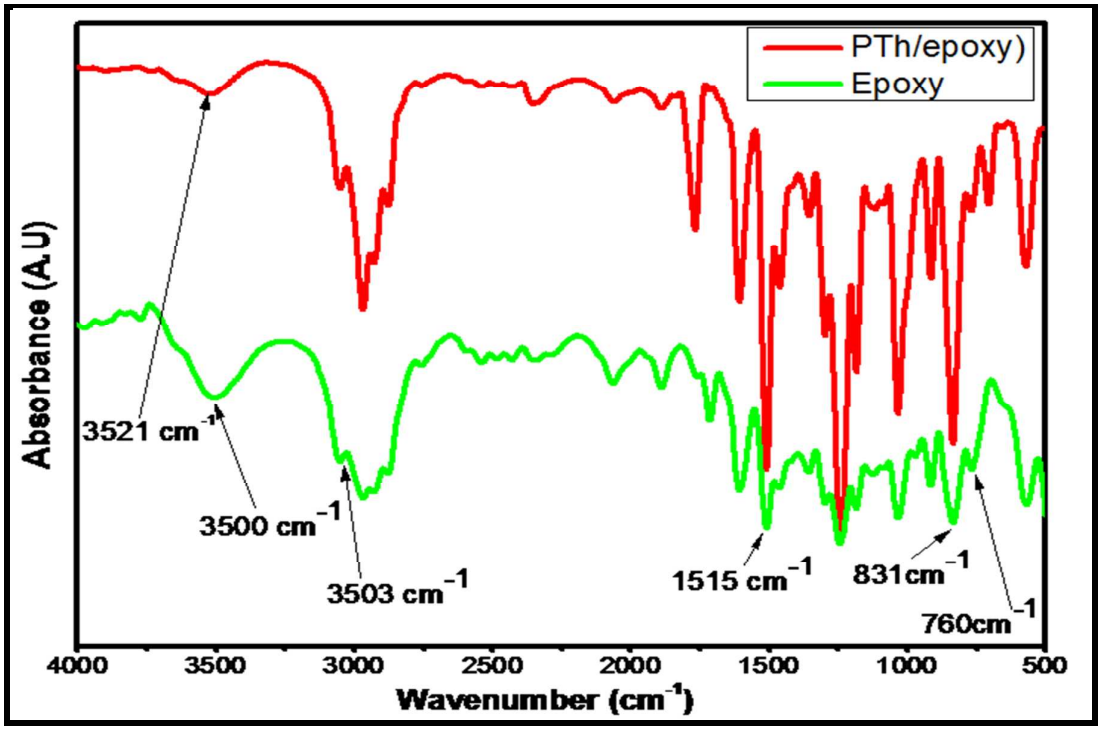

Figure 1(b) FT-IR spectra of PTh dispersed epoxy and DGEBA epoxy.

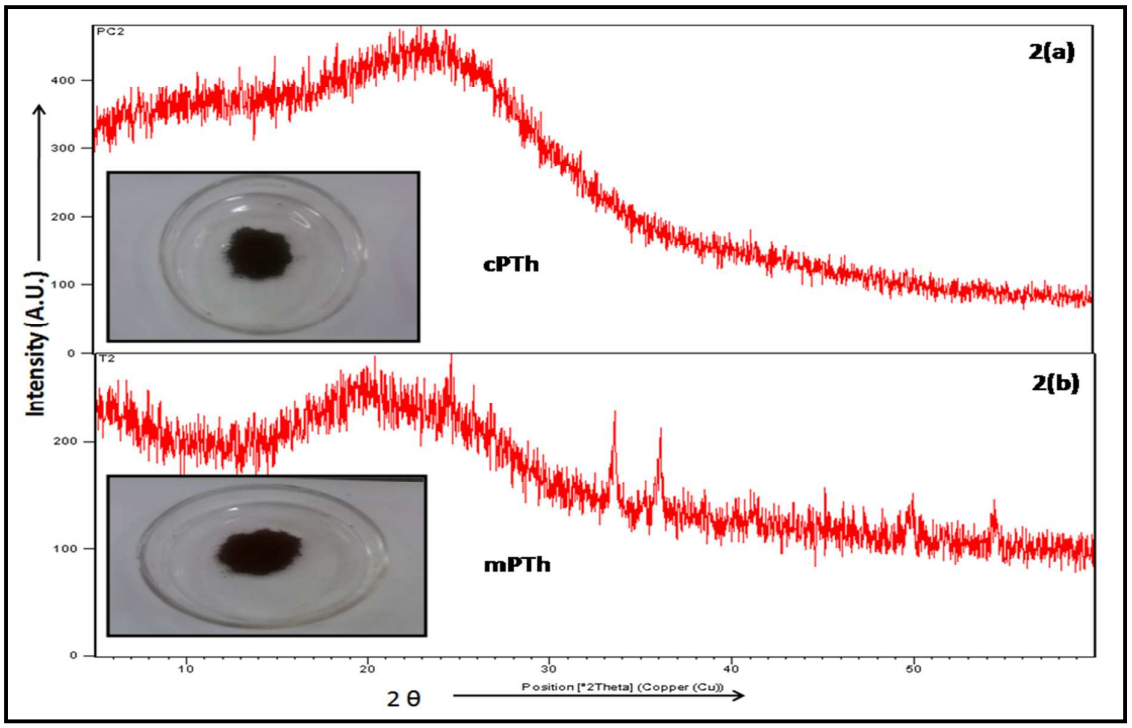

Figure 2 X-ray diffraction patterns of (a) cPTh nanoparticles (b) mPTh nanoparticles.

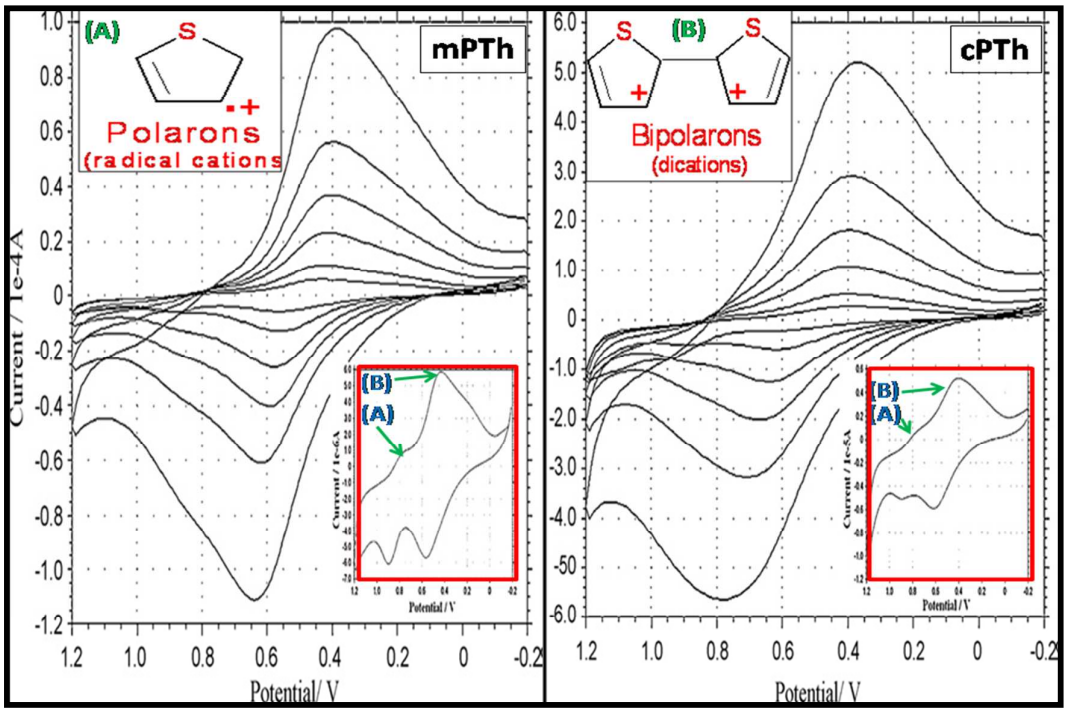

Figure 3 Cyclic voltammograms of mPTh and cPTh nanoparticles at different scan rates.

.

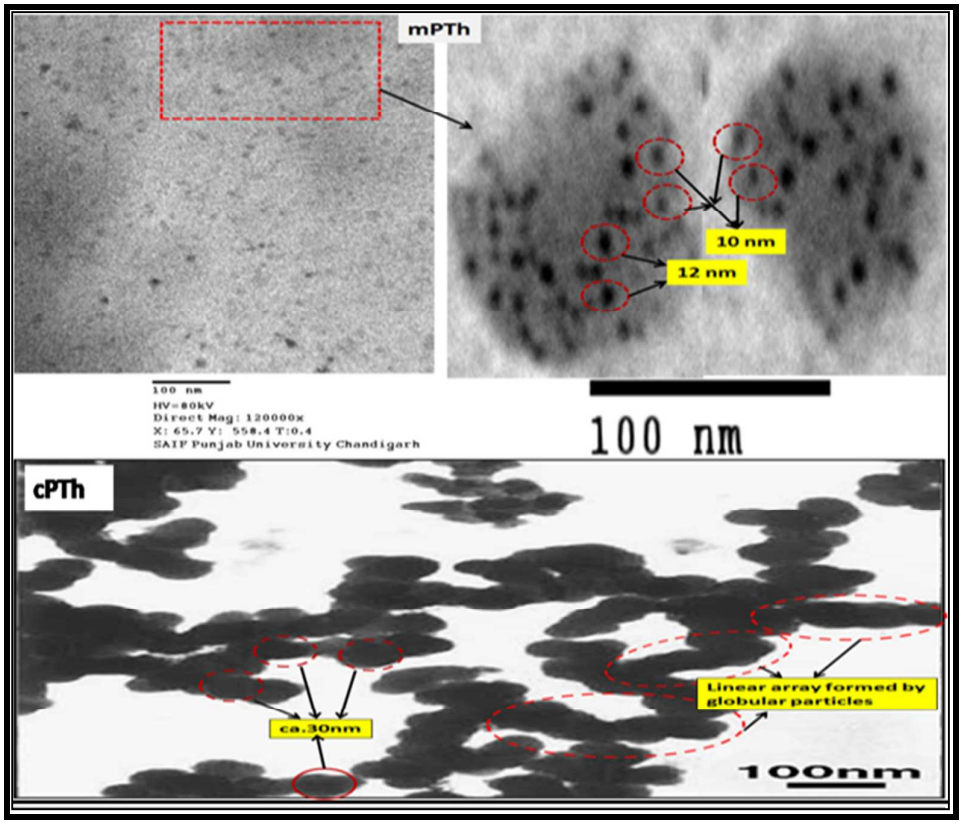

Figure 4(a) TEM micrographs of well dispersed mPTh, cPTh nanoparticles in water

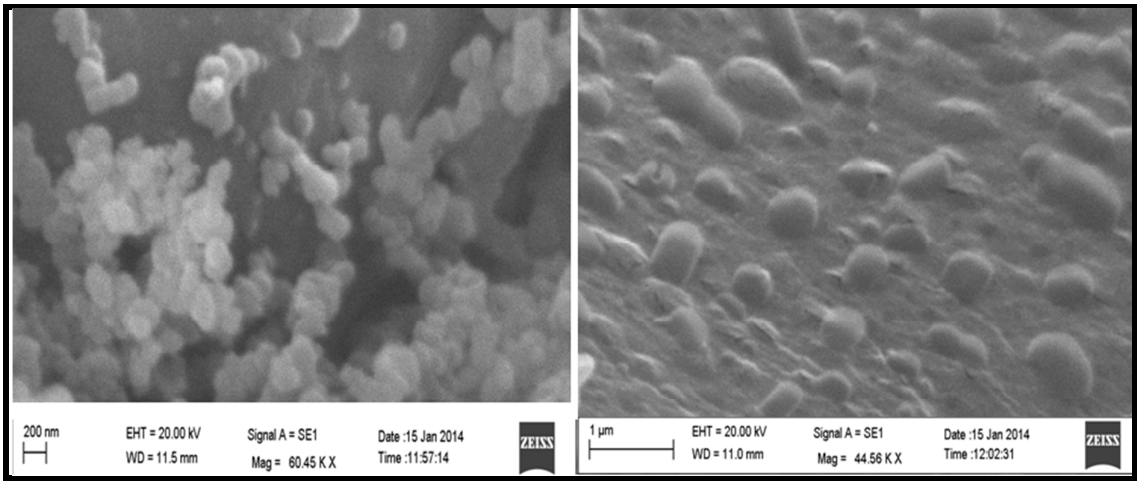

Figure 4(b) SEM images showing the formation of (i) nano-spheres of mPTh nanoparticles (ii) nano-particles of cPTh having spherical and elongated morphology.

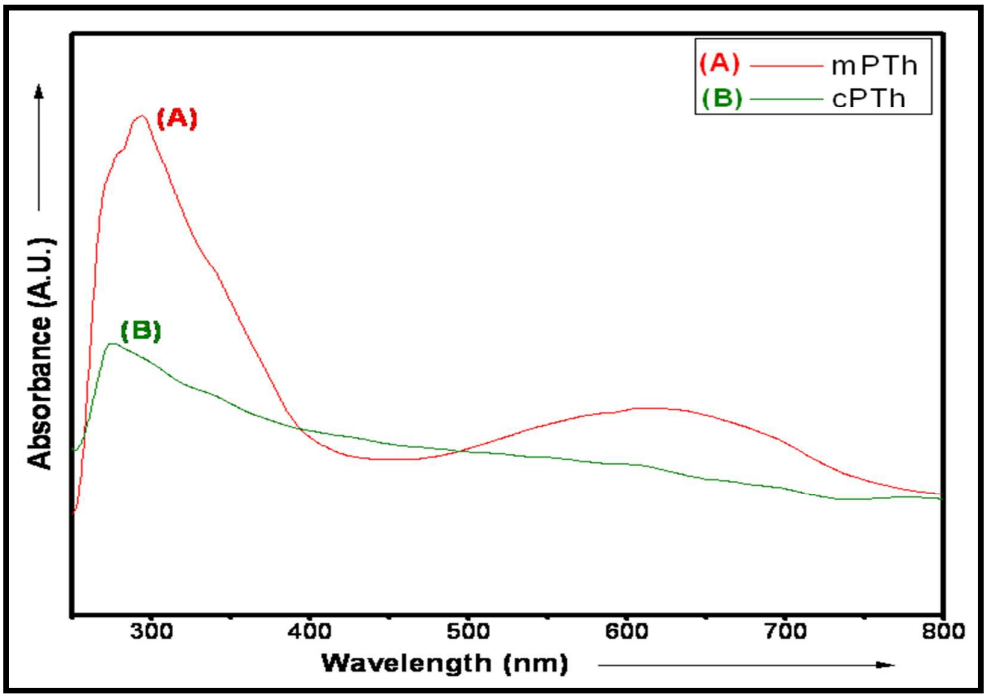

Figure 5 UV-vis spectra of (A) mPTh and (B) cPTh nanoparticles in DMSO.

.

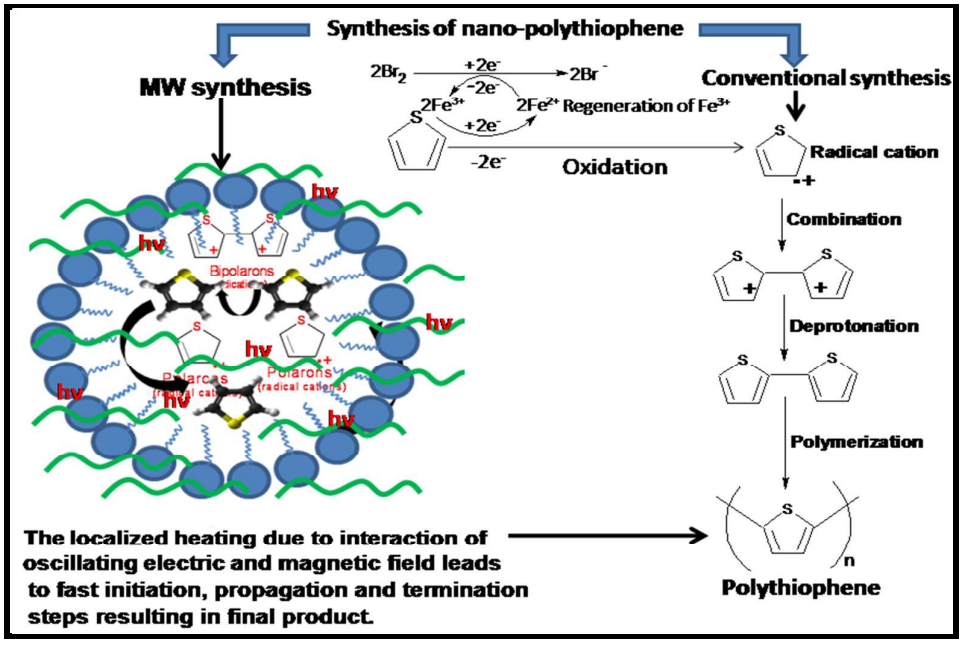

Scheme 1 Mechanism showing the steps involved during the synthesis of Polythiophene in MW and conventional surfactant assisted synthesis.

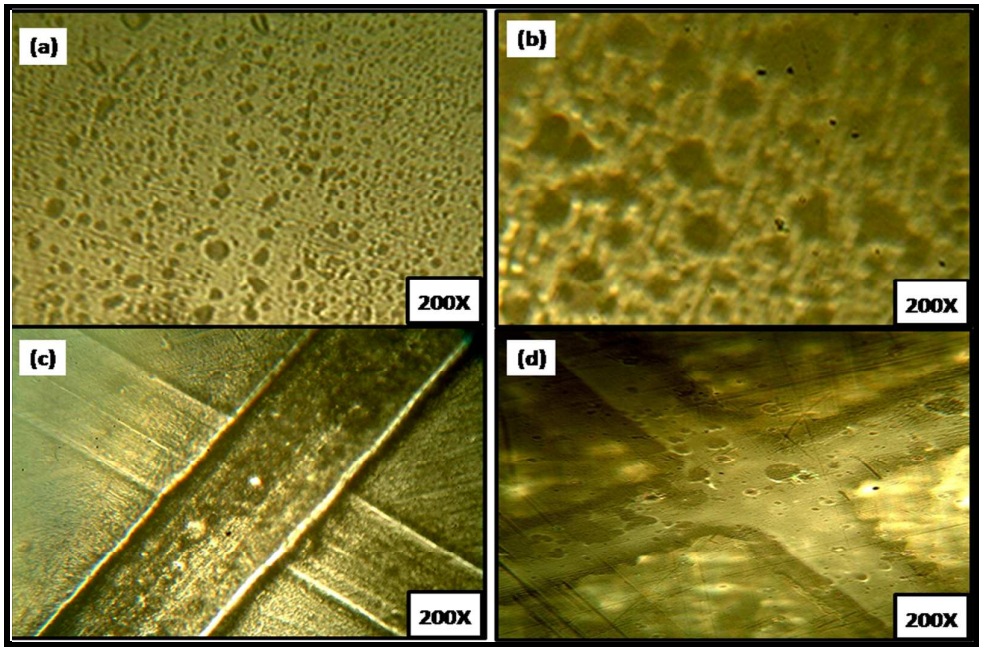

Figure 6 Optical micrographs of (a) mPTh-epoxy-PA coating (b) cPTh-epoxy-PA coating (c) Cross hatched mPTh-epoxy-PA coating and (d) Cross hatched cPTh-epoxy-PA coating.

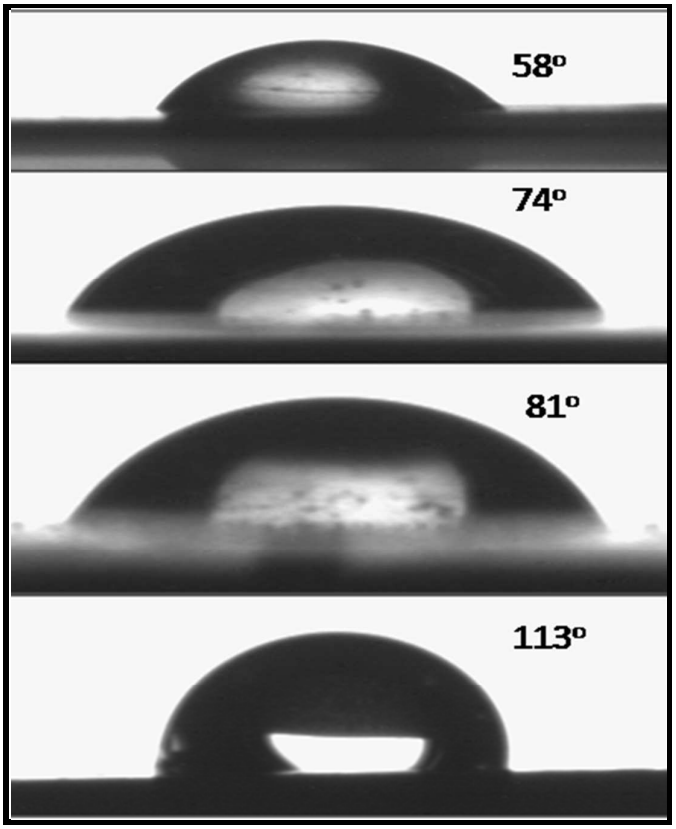

Figure 7 Contact angle measurements of (a) bare CS (b) epoxy coated CS (c) cPTh-epoxy coated CS (d) mPTh-epoxy coated CS

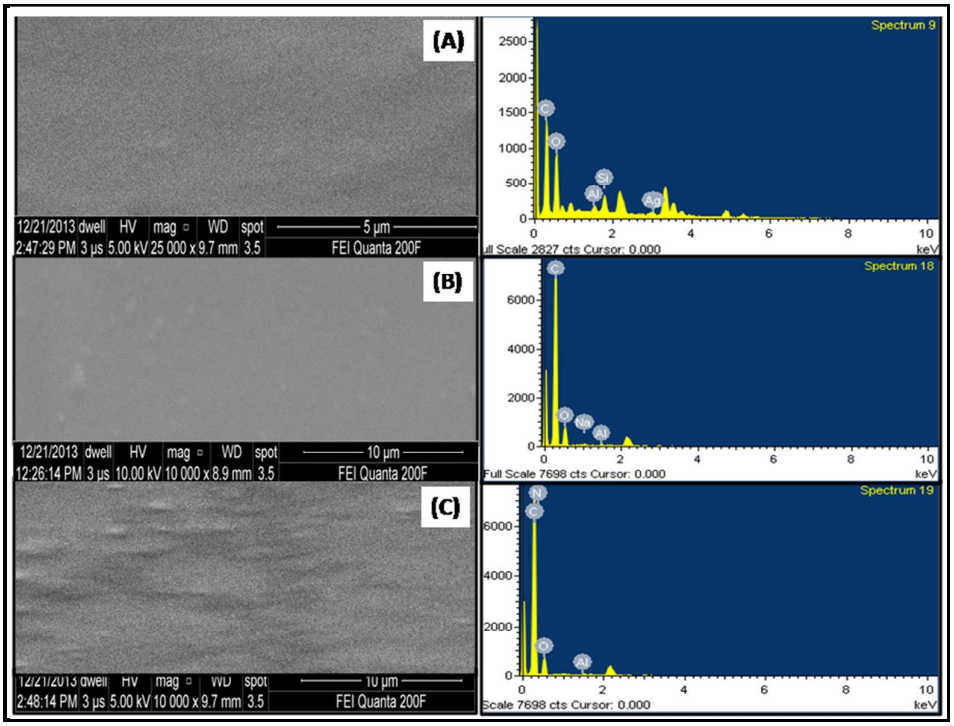

Figure 8 (a) SEM/EDAX studies of (a) epoxy coated CS (b) cPTh-epoxy-PA coated CS and (c) mPTh-epoxy-PA coated CS before salt mist test.

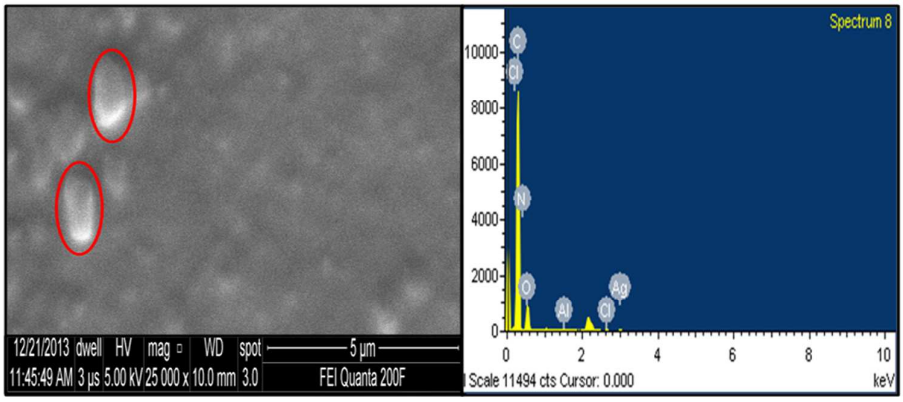

Figure 8 (d) SEM/EDAX studies of mPTh-epoxy-PA coated CS after salt mist test.

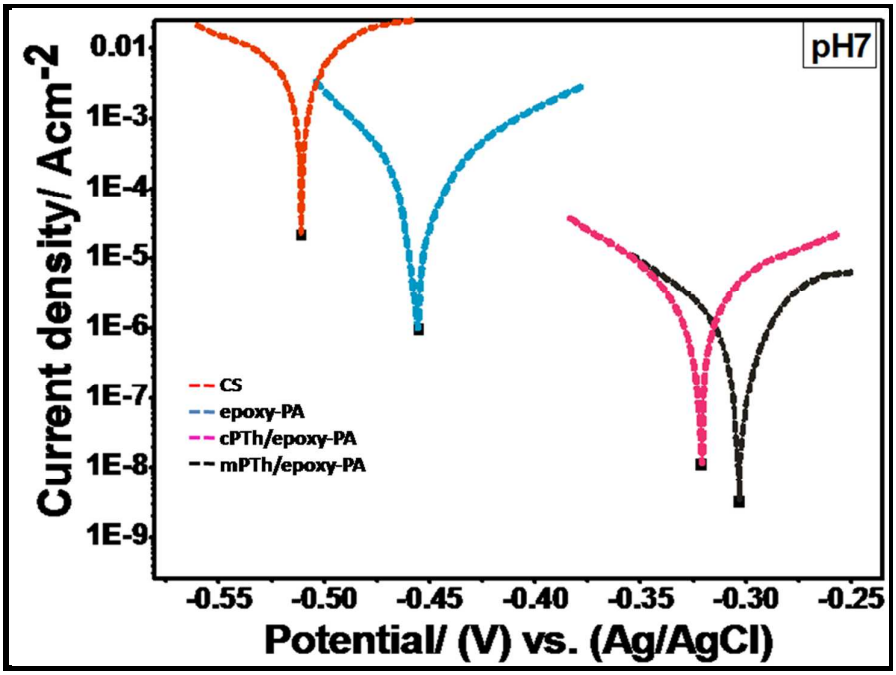

Figure 9(a) Potentiodynamic polarisation curves of uncoated CS, epoxy-PA, cPTh-epoxy-PA and mPTh-epoxy-PA in 3.5% NaCl media of pH=7.

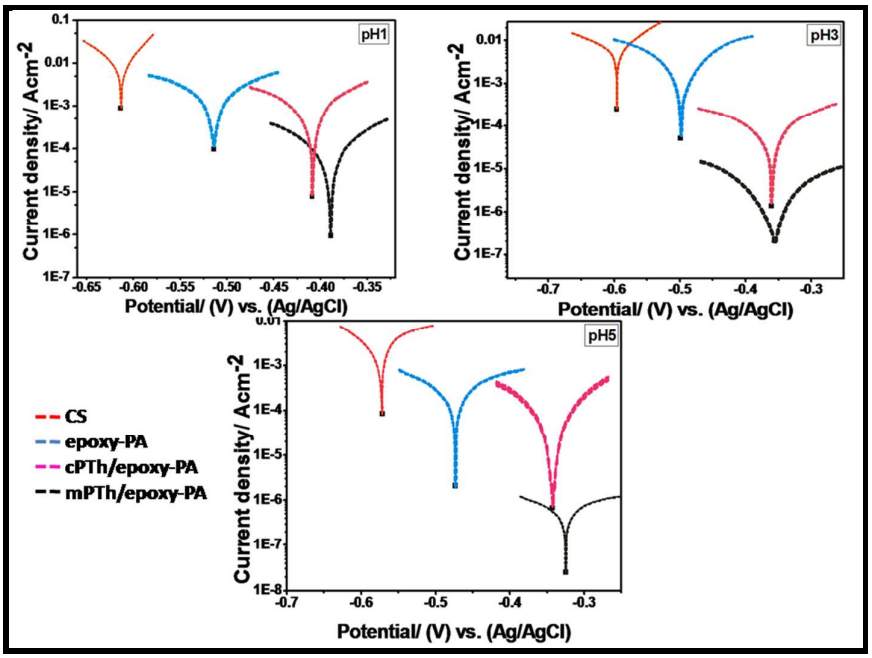

Figure 9(b) Potentiodynamic polarisation curves of bare CS, epoxy-PA, cPTh-epoxy- PA and mPTh-epoxy-PA in 3.5% NaCl media of varying (a) pH = 1 (b) pH = 3 and (c) pH = 5.

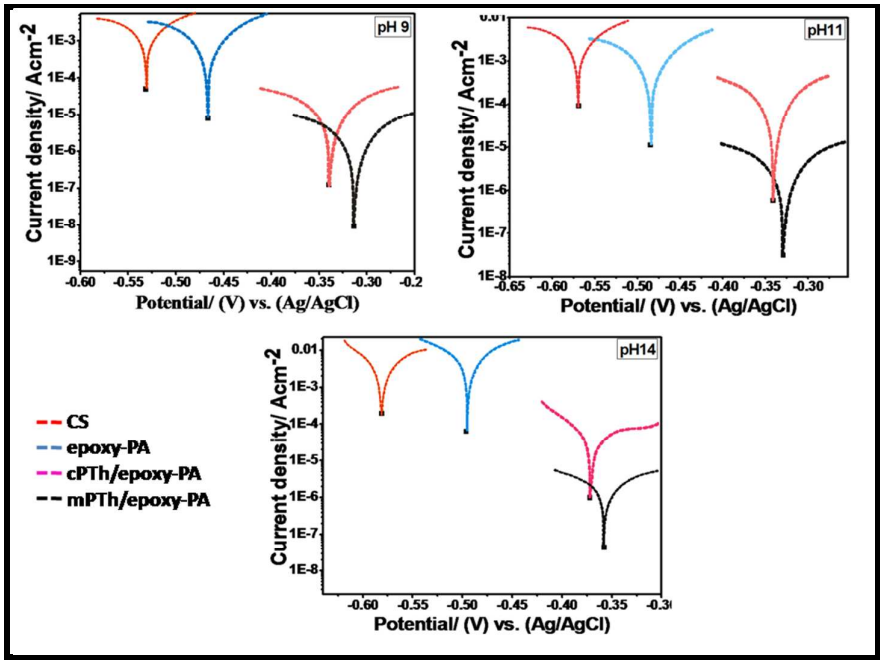

Figure 9(c) Potentiodynamic polarisation curves of uncoated CS, epoxy-PA, cPTh-epoxy-PA and mPTh-epoxy-PA in 3.5% NaCl media of varying (a) pH = 9 (b) pH = 12 and (c) pH =14.

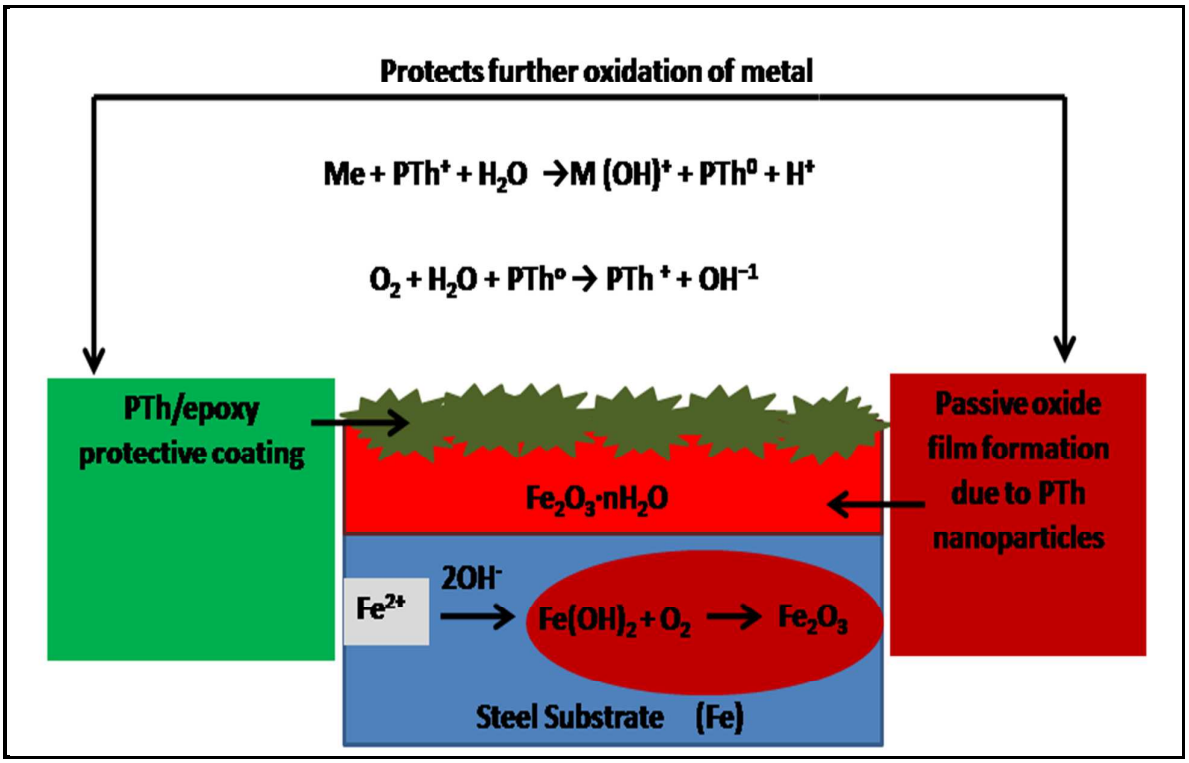

Scheme 2. Passive oxide film formation in PTh-epoxy-PA nanocomposite coatings.